micromachines

MDPI

Article

Nested Constraint Dynamic Modeling and Cooperative Control of Reconfigurable Micro Modular Robotic Vehicle Swarms

Xiao Su [1], Duanling Li [1,2,*], Fengkun Xu [1] and Jin Huang [3]

[1] School of Intelligent Engineering and Automation, Beijing University of Posts and Telecommunications, Beijing 100083, China; suxiao@bupt.edu.cn (X.S.); fengkunxu@163.com (F.X.)
[2] School of Mechanical and Electrical Engineering, Shaanxi University of Science and Technology, Xian 710021, China
[3] School of Vehicle and Mobility, Tsinghua University, Beijing 100080, China; huangjin@tsinghua.edu.cn
* Correspondence: liduanling_bupt@163.com

Abstract

Reconfigurable miniature modular robotic swarms realize flexible payload transportation by the serial assembly of micro vehicle modules. Strong dynamic coupling and unsynchronized motion among interconnected modules bring prominent challenges to the stable cooperative operation of micro-robotic transport systems. To tackle modeling and coordination control challenges of scalable micro modular robots with variable chassis structures, this paper develops a hierarchical nested constraint-following modeling and cooperative control framework based on UK analytical dynamics, with distinct mathematical and computational advances over conventional monolithic modeling approaches. Each miniature module is equipped with an integrated steering micro chassis and embedded controllers for real-time motion computation. First, an underactuated nonlinear dynamic model for each individual unit is built without redundant auxiliary variables. Based on this unit model, the proposed framework supports swarm system modeling for transportation swarms composed of an arbitrary number of modules. Second, inter-module geometric constraints are transformed into second-order acceleration equations. Moore–Penrose pseudoinverse analytically solves constraint forces, enabling recursive nested full-system modeling for n connected modules. From a computational perspective, the recursive nested architecture eliminates the need to reconstruct global mass and constraint matrices from scratch when the swarm configuration changes, which significantly reduces modeling complexity and enables scalable dynamic computation. Third, global trajectory tracking missions are recursively decomposed into independent constraint-following subtasks for each module, with a damping correction term embedded to eliminate initial tracking errors. Numerical simulations with four serially connected miniature modular robot units demonstrate that trajectory tracking errors converge to near zero within 0.5s. Compared with the LQR baseline controller, the proposed approach achieves a lower peak deviation and a substantially reduced cumulative tracking error. When subject to external torque disturbance, the system maintains satisfactory heading synchronization and rapidly recovers steady-state control outputs, verifying favorable disturbance-rejection performance. This work offers a unified modeling and coordination-control solution for reconfigurable micro robotic transport platforms, supporting micro-robotics haulage research.

Keywords: micro modular vehicle; multi-micro-robot cooperative control; miniature embedded controller; constraint-following dynamics

Check for updates

Academic Editor: Duc Truong Pham

Received: 24 September 2026
Revised: 29 October 2026
Accepted: 29 October 2026
Published: 30 October 2026

Copyright: © 2026 by the authors. Licensee MDPI, Basel, Switzerland. This article is an open access article distributed under the terms and conditions of the Creative Commons Attribution (CC BY) license.

1. Introduction

Reconfigurable miniature modular robotic vehicle swarms [1] have emerged as a novel flexible transportation platform in micro-robotics haulage engineering. Different from traditional integrated heavy-duty vehicles with fixed chassis configurations, such micro robotic systems realize variable-scale payload transportation and adaptive mobility through the serial assembly of standardized micro vehicle modules. This modular reconfigurable architecture possesses prominent advantages including flexible structure assembly, scalable load capacity, and adaptive environmental adaptability, which enables unique application prospects in narrow-space cargo transportation, micro-area material handling, and special-scene mobile operation missions. Nevertheless, the serial connection and collaborative motion of multiple miniature modules introduce complex dynamic coupling effects and asynchronous motion characteristics between interconnected units. These inherent characteristics easily induce vehicle body jitter and poor motion synchronization during transportation, bringing challenges to the stable operation of micro robotic transport systems and severely restricting the practical engineering application of modular micro-robot swarms.

Vehicle dynamic modeling and cooperative motion control constitute the core theoretical foundation for ensuring stable tracking and safe operation of mobile robotic and vehicle systems. For traditional integrated vehicles and fixed-structure haulage equipment, relevant modeling and control theories have formed a relatively complete technical system, which mainly rely on multi-body dynamics and physical-mechanism-based modeling for vehicles with fixed chassis layouts and centralized drive configurations [2–7]. Scholars have carried out extensive studies covering heavy-vehicle stability, multi-wheel vehicle dynamics, multi-axle and articulated vehicle modeling, as well as reconfigurable modeling concepts for articulated vehicles.

Nevertheless, these existing theories show evident limitations when applied to reconfigurable micro-modular robotic vehicle swarms. First, most conventional vehicle dynamic models are built for fixed chassis structures and fixed degrees of freedom, which cannot adapt to micro-modular swarms with arbitrary module numbers and variable connection modes. Second, many existing approaches simplify multi-actuator coupling and ignore strong dynamic coupling as well as motion-synchronization discrepancies between serially connected micro-modules, resulting in unsatisfactory modeling accuracy for reconfigurable swarm systems. Third, the majority of cooperative control strategies for multi-body vehicles adopt centralized frameworks, lacking hierarchical decoupling and recursive solving capacity required by variable-scale modular clusters. Moreover, the complex nonlinear characteristics of micro-modules, such as tire-slip effects and load transfer, are rarely fully considered, further restricting tracking accuracy for micro-robotic transportation platforms.

Aiming at the above modeling and cooperative control bottlenecks of scalable reconfigurable micro modular robotic vehicles with variable chassis structures, this paper proposes a hierarchical nested constraint-following modeling and cooperative control framework based on the Udwadia–Kalaba (UK) [8–12] analytical dynamics theory. Different from traditional numerical modeling and centralized control methods, the proposed framework abandons redundant auxiliary variables and realizes unified dynamic modeling and scalable cooperative control for arbitrarily assembled micro module swarms. Each miniature robot module is equipped with an integrated steering micro chassis and embedded controller to support high-precision real-time motion computation. Specifically, an underactuated nonlinear dynamic model for each individual unit is first established to accurately describe the intrinsic motion law of single micro modules. Leveraging the nested constraint-following mechanism, the overall swarm system model can be constructed for transportation systems with arbitrary module quantities. On this basis, inter-module geometric assembly constraints are converted into second-order acceleration constraint

equations, and the Moore–Penrose pseudoinverse algorithm is adopted to analytically solve system constraint forces, realizing recursive nested full-system dynamic modeling for arbitrarily connected n-module swarms. Furthermore, global trajectory tracking missions are recursively decomposed into independent constraint-following subtasks for each module, and a damping correction term is embedded in the control law to eliminate initial tracking errors and realize high-precision synchronous cooperative motion of the swarm system.

It is worthwhile to clarify the novelty and incremental advances of the present work relative to existing UK-based studies and our group's prior publications. Previous UK-driven multi-body dynamics mainly focus on fixed-topology mechanical systems or single-vehicle systems, where system-level mass and constraint matrices need to be fully reconstructed whenever the system configuration changes, leading to sharply growing computational burden with expanding system scale. Our earlier work investigated nested closed-form dynamics for modular electric vehicles, yet it did not address the underactuated characteristics of miniature modular robotic units, nor the recursive decomposition of global trajectory-tracking tasks for serially connected swarm clusters. Distinct from those prior efforts, this paper proposes a hierarchical nested recursive modeling strategy tailored specifically for serially assembled underactuated micro-modular robot swarms, with core mathematical and computational contributions as follows. The overall system dynamics are hierarchically decomposed into individual-unit underactuated dynamics and pairwise inter-module geometric constraints. New modules can be incorporated by only appending local constraint relations rather than rebuilding full-system matrices from scratch, which enables recursive dynamic modeling for arbitrarily connected modular units and suppresses the growth of computational complexity. Moreover, global swarm trajectory-tracking objectives are recursively decomposed into distributed constraint-following subtasks for each robot module, with a damping correction term embedded to suppress initial synchronization errors. These features collectively advance the state-of-the-art for reconfigurable micromodular swarm transportation by extending UK constraint-following theory to variable-scale underactuated serial robotic assemblies, and provide a computationally scalable solution for reconfigurable micro transport platforms.

Comparative simulation experiments of four serially connected micro modular robots verify the effectiveness and superiority of the proposed method. Compared with the LQR(Linear Quadratic Regulator) baseline controller, the developed framework achieves lower peak and cumulative tracking error. The results show that the system trajectory tracking error converges to zero within 0.5s, and the module control forces and moments can quickly reach stable steady states. Moreover, the system maintains stable cooperative motion and fast recovery for control outputs under external torque disturbance, demonstrating favorable disturbance-rejection capability. This work constructs a unified modeling and coordination control solution for reconfigurable micro robotic transport platforms, which effectively solves the dynamic coupling and asynchronous motion problems of modular swarm systems and provides novel theoretical and technical support for the research and engineering application of micro-robotics haulage systems.

2. Fundamental Udwadia-Kalaba Constraint-Following Dynamics Framework

UK analytical dynamics theory has delivered a landmark generalized motion solution for multi-body mechanical systems subjected to holonomic and nonholonomic constraints over the past three decades, offering a concise analytical tool to explicitly resolve constraint forces without extra Lagrange multipliers or redundant state variables. This theoretical foundation lays the core mathematical support for the nested dynamic modeling of arbitrarily assembled reconfigurable micro modular robotic vehicle swarms in this work.

Assume the target multi-body system consists of rigid bodies and discrete particles, with n-dimensional generalized coordinates $q \in R^n$, generalized velocity vector $\dot{q} \in R^n$, and generalized acceleration vector $\ddot{q} \in R^n$. The governing motion equation of the unconstrained baseline system is formulated as:

$$M(q(t), t)\ddot{q}(t) = Q(q(t), \dot{q}(t), t), \tag{1}$$

where $t \in R$ is the independent variable time. In addition, $M \in R^{n \times n}$ is the inertia matrix, $Q \in R^n$ is the impressed (or applied) force plus all Coriolis/centrifugal and gravitational terms. Both matrix-valued functions $M(\cdot)$ and vector-valued functions $Q(\cdot)$ satisfy continuous smoothness assumptions.

A set of consistent constraint relations is imposed on the unconstrained baseline system. Assume $m(m \leq n)$ independent constraint equations of the following form are applied to the system:

$$\sigma_i(q, \dot{q}, t) = 0, i = 1, 2, \cdots, m, \tag{2}$$

where mapping $\sigma(\cdot) : R^n \times R^n \times R \to R$, $\sigma_i(\cdot)$ exhibits sufficient smoothness to support required time differentiation operations.

The constraint set covers standard holonomic and nonholonomic constraint types. All constraint relations are assumed to possess adequate differentiability with respect to time t, which permits transformation into second-order acceleration-domain formulations:

$$A(q, \dot{q}, t)\ddot{q} = b(q, \dot{q}, t), \tag{3}$$

where $A \in R^{m \times n}$ denotes the constraint matrix, and $b \in R^{m \times 1}$ represents an m-dimensional vector.

Due to the presence of constraints, additional 'generalized forces of constraints' should be imposed on the system. Thus, the explicit equation of motion for the constrained system can be expressed as:

$$M(q(t), t)\ddot{q}(t) = Q(q(t), \dot{q}(t), t) + Q^e(q(t), \dot{q}(t), t), \tag{4}$$

where $Q^e \in R^n$ denotes supplementary generalized forces generated by holonomic and nonholonomic constraint restrictions. The core mathematical objective lies in the analytic resolution of the constraint force vector Q^e. Based on Gauss's principle of least constraint, Udwadia and Kalaba derived an explicit closed-form expression for constraint force vectors as follows:

$$Q^e = M^{\frac{1}{2}}\left(AM^{-\frac{1}{2}}\right)^{+}\left(b - AM^{-1}Q\right), \tag{5}$$

where the superscript '+' designates the Moore-Penrose generalized matrix inverse operation.

The Moore–Penrose generalized inverse of the constraint matrix A occupies a pivotal role in characterizing constrained system motion behaviors. Explicit motion equations governing constrained dynamic systems can be derived without prior knowledge of matrix A' s rank, which facilitates deeper physical interpretation of constrained motion mechanics. The Moore–Penrose generalized inverse A^+ uniquely satisfies the following four conditions:

$$AA^+A = A \tag{6}$$

$$A^+AA^+ = A \tag{7}$$

$$AA^+ = \left(AA^+\right)^T \tag{8}$$

$$A^{+}A = \left(A^{+}A\right)^{T}. \tag{9}$$

Combining the above constraint force derivation, the explicit closed-form motion equation governing full-state evolution of constrained multi-body systems reads:

$$M\ddot{q} = Q + M^{\frac{1}{2}}\left(AM^{-\frac{1}{2}}\right)^{+}(b - Aa), \tag{10}$$

$$\ddot{q} = a + M^{-\frac{1}{2}}\left(AM^{-\frac{1}{2}}\right)^{+}(b - Aa), \tag{11}$$

where $a = M^{-1}Q$.

Equation (10) is recognized as the fundamental motion equation for constrained mechanical systems. The formulation exhibits concise mathematical structure and delivers an efficient analytic tool for processing arbitrary holonomic and nonholonomic constraint relations, which constitutes the core theoretical foundation for subsequent nested constraint modeling of interconnected micro modular vehicle swarms.

3. Theory of Constraints Analysis

Multi-level constraints are required for the modeling and control of reconfigurable miniature modular robots. When multiple constraints are sequentially applied to the dynamic system under the cascading constraint mechanism, the constraint forces introduced by newly added constraints disturb the original system motion and often render previous constraints unsatisfied. Conventional dynamic consistency conditions merely enable passive verification of constraint preservation, lacking the capability to actively design control inputs for concurrent satisfaction of all multi-level constraints. To resolve such conflicts caused by cascaded multi-constraint superposition, the constraint-following control paradigm offers a standardized solution. This paradigm regards the mechanical system as an unconstrained baseline model, embeds all control targets into dynamic formulations as additional constraint equations, and computes the required control input analytically through the closed-form UK equation. By uniformly converting all control objectives into acceleration constraints, the framework is natively applicable to complex motion control tasks with simultaneous multiple constraints and sequentially cascaded constraint stacking.

Consider two unconstrained systems, as follows:

$$S_i : M_i(q_i(t), t)\ddot{q}_i(t) = Q_{0i}(q_i(t), \dot{q}_i(t), t)(i = 1, 2.) \tag{12}$$

where $t \in R$ is the independent variable time, $q_i \in \mathbf{R}^{n_i}$ is the position vector, $\dot{q} \in \mathbb{R}^n$ is the velocity vector, and $\ddot{q}_i \in \mathbf{R}^{n_i}$ is the acceleration vector. In addition, $M_i \in \mathbf{R}^{n_i \times n_i}$ is the inertia matrix, $Q_{0i} \in \mathbf{R}^{n_i}$ is the impressed (or applied) force plus all Coriolis/centrifugal and gravitational terms.

The combined mechanical system is

$$S : M\ddot{q} = Q_0 \tag{13}$$

where $q = [q_1, q_2]^T, q \in \mathbf{R}^n, n = n_1 + n_2, M = diag(M_1, M_2), M \in \mathbf{R}^{n \times n}, Q_0 = [Q_{01}, Q_{02}]^T, Q_0 \in \mathbf{R}^n$. We consider the following three constraints $C_1, C_2, \mathbf{C}$ for S_1, S_2, and S, respectively:

(i) $C_1 : \bar{A}_1\ddot{q}_1 = \bar{b}_1$. Here $\bar{A}_1 \in \mathbf{R}^{m_1 \times n_1}, \bar{b}_1 \in \mathbf{R}^{m_1}$.

(ii) $C_2 : \bar{A}_2\ddot{q}_2 = \bar{b}_2$. Here $\bar{A}_2 \in \mathbf{R}^{m_2 \times n_2}, \bar{b}_2 \in \mathbf{R}^{m_2}$.

(iii) $\mathbf{C} : \bar{\mathbf{A}}\ddot{q} = \bar{\mathbf{b}}$. Here $\bar{A} \in \mathbf{R}^{l \times n}, \bar{b} \in \mathbf{R}^{l}$. The matrix $\bar{A}$ can be partitioned as

$$\bar{\mathbf{A}} = \begin{bmatrix} \bar{\mathbf{A}}_{11} & \bar{\mathbf{A}}_{12} \\ \bar{\mathbf{A}}_{21} & \bar{\mathbf{A}}_{22} \end{bmatrix}. \tag{14}$$

Here, $\bar{\mathbf{A}}_{11} \in \mathbf{R}^{l_1 \times n_1}, \bar{\mathbf{A}}_{12} \in \mathbf{R}^{l_1 \times n_2}, \bar{\mathbf{A}}_{21} \in \mathbf{R}^{l_2 \times n_1}, \bar{\mathbf{A}}_{22} \in \mathbf{R}^{l_2 \times n_2}, l_1 + l_2 = l$. Notice that C_1 is applied to S_1, C_2 is applied to S_2, and $\mathbf{C}$ is applied to S.

Theorem 1. *Consider the mechanical systems S_1, S_2 and the combined mechanical system S. Suppose the constraint C_1 is imposed on S_1, followed by C_2 imposed on S_2. This is followed by the constraint $\boldsymbol{C}$ imposed on S. Then, the combined system S meets all the constraints C_1, C_2 if*

$$\bar{\boldsymbol{A}}_1 M^{-\frac{1}{2}} (\bar{\boldsymbol{A}}_2 M^{-\frac{1}{2}})^+ (\bar{\boldsymbol{b}}_2 - \bar{\boldsymbol{A}}_2 M^{-1} Q_1) = 0 \tag{15}$$

$$\bar{\boldsymbol{A}}_2 M^{-\frac{1}{2}} (\bar{\boldsymbol{A}} M^{-\frac{1}{2}})^+ (\bar{\boldsymbol{b}} - \bar{\boldsymbol{A}} M^{-1} Q_2) = 0 \tag{16}$$

$$\bar{\boldsymbol{A}}_1 M^{-\frac{1}{2}} (\bar{\boldsymbol{A}} M^{-\frac{1}{2}})^+ (\bar{\boldsymbol{b}} - \bar{\boldsymbol{A}} M^{-1} Q_2) = 0 \tag{17}$$

The proof of Theorem 1 is presented in Appendix A.

4. An Expanded Approach to Nested Constraint Modeling

According to the hierarchical properties of the UK equation, a particle, rigid body system, or other multibody system can be decomposed into several subsystems, and a multibody system model can be established based on the constraint relationships among each subsystem [13].

Based on Equation (5), the constraint force Q^e is determined by Q. This formulation enables the equation of motion to be expressed in a cascading manner as additional constraints are imposed on the system. Suppose the unconstrained system:

$$M(q,t)\ddot{q} = Q_0(q,\dot{q},t), \tag{18}$$

is subject to the constraint $A_1(q,t)\ddot{q} = b_1(q,\dot{q},t)$, then one can formulate the equation of motion as

$$M(q,t)\ddot{q} = Q_1(q,\dot{q},t), \tag{19}$$

where

$$Q_1 = Q_0 + Q_1^e, \tag{20}$$

$$Q_1^e = M^{\frac{1}{2}} \left(A_1 M^{-\frac{1}{2}} \right)^+ \left(b_1 - A_1 M^{-1} Q_0 \right). \tag{21}$$

One can interpret Equation (19) as being in the same form as Equation (18), an unconstrained mechanical system. Next, suppose there is an additional constraint, $A_2(q,t)\ddot{q} = b_2(q,\dot{q},t)$, added to the system motion. Then, one can formulate the equation of motion as:

$$M(q,t)\ddot{q} = Q_2(q,\dot{q},t), \tag{22}$$

where

$$Q_2 = Q_1 + Q_2^e, \tag{23}$$

$$Q_2^e = M^{\frac{1}{2}} \left(A_2 M^{-\frac{1}{2}} \right)^+ \left(b_2 - A_2 M^{-1} Q_1 \right). \tag{24}$$

This iterative process can be implemented with additional constraints. Now, letting the constraints be $A_i(q,t)\ddot{q} = b_i(q,\dot{q},t)$, where $(i = 1, 2, \ldots, l)$, the equation of motion for the constrained system is given by:

$$M(q,t)\ddot{q} = Q_i(q,\dot{q},t), \tag{25}$$

where

$$Q_i = Q_{i-1} + Q_i^e, \tag{26}$$

$$Q_i^e = M^{\frac{1}{2}}\left(A_i M^{-\frac{1}{2}}\right)^+\left(b_i - A_i M^{-1} Q_{i-1}\right). \tag{27}$$

A dynamic modeling method based on nested constraint design, utilizing the UK equation, is proposed. The multi-rigid body intelligent system is envisaged as a composite of multiple module subsystems that correspond to each other. Starting from the unconstrained dynamic model of these modular units, corresponding constrained kinematic models are embedded to develop a constrained dynamic model. Building on this, a new constrained kinematic model is integrated with other modules to establish a dynamic model for the reassembly module. This iterative process facilitates the nested modeling of multi-agent transportation system dynamics. Through the modeling of each module independently and the leveraging of nested constraint relationships, the overall model is enhanced with the capability for modules to be freely added, removed, or replaced without impacting other parts, thus significantly enhancing the adaptability of the overall system.

Assuming a multibody system is composed of k_0 basic units, these units can be combined into k_1 first-level subsystems based on their kinematic or constraint relationships. The constraint relationships are unique and non-overlapping, indicating that a basic unit can only contribute to one first-level subsystem and cannot simultaneously participate in multiple first-level subsystems. In a similar fashion, k_1 first-level subsystems can form k_2 second-level subsystems; likewise, $k_n - 1$ subsystems at the $n-1$ level can develop into k_n subsystems at the n level; ultimately, these k_n subsystems at the n-level constitute the entire multibody system.

The specific process of the dynamic modeling method, based on hierarchical constraint design, proceeds as follows: First, establish the dynamic models for each basic unit; the motion equations of these units can be expressed as:

$$M_{j0}(q_{j0}, t)\ddot{q}_{j0} = Q_{j0}(q_{j0}, \dot{q}_{j0}, t), \tag{28}$$

where $j = 1, 2, \ldots k_0$, M_{j0} is the mass matrix of $n_{j0} \times n_{j0}$, q_{j0} is n_{j0}-dimensional state vector, Q_{j0} is n_{j0}-dimensional generalized force applied to the system.

The constraints imposed on the system are expressed in the form of matrix equations as follows:

$$A_{j0}(q_{j0}, \dot{q}_{j0}, t)\ddot{q}_{j0} = b_{j0}(q_{j0}, \dot{q}_{j0}, t), \tag{29}$$

where A_{j0} expresses the constraint matrix of $m_{j0} \times n_{j0}$, b_{j0} is n_{j0}-dimensional vector.

The motion equation of a constrained system can be described as:

$$\begin{aligned} M_{j0}(q_{j0}, t)\ddot{q}_{j0} &= Q_{j0}(q_{j0}, \dot{q}_{j0}, t) + Q_{j0}^e(q_{j0}, \dot{q}_{j0}, t) \\ &=: \hat{Q}_{j0}(q_{j0}, \dot{q}_{j0}, t), \end{aligned} \tag{30}$$

where Q_{j0}^e is n_{j0}-dimensional constraint torque matrix; the display expression is:

$$Q_{j0}^e = M_{j0}^{\frac{1}{2}}\left(A_{j0} M_{j0}^{-\frac{1}{2}}\right)^+\left(b_{j0} - A_{j0} M_{j0}^{-1} Q_{j0}\right). \tag{31}$$

Secondly, following the development of dynamic models for each basic unit, unique and non-overlapping constraint relationships are employed to create k_1 primary level subsystems. These constraints are expressed as matrix equations:

$$A_{j1}(q_{j1}, \dot{q}_{j1}, t)\ddot{q}_{j1} = b_{j1}(q_{j1}, \dot{q}_{j1}, t), \tag{32}$$

where $j = 1, 2, \ldots k_1$, A_{j1} expresses the constraint matrix of $m_{j1} \times n_{j1}$, b_{j1} is m_{j1}-dimensional vector, q_{j1} is an n_{j1}-dimensional state vector, composed of state variables aggregated from various basic units within its first-level subsystem.

The motion equation of the first-level subsystem, derived from the constraint relationships in Equation (32), is described as follows:

$$\begin{aligned} M_{j1}\left(q_{j1}, t\right)\ddot{q}_{j1} &= Q_{j1}\left(q_{j1}, \dot{q}_{j1}, t\right) + Q_{j1}^{e}\left(q_{j1}, \dot{q}_{j1}, t\right) \\ &= Q_{j1}\left(q_{j1}, \dot{q}_{j1}, t\right) + M_{j1}^{\frac{1}{2}}\left(A_{j1}M_{j1}^{-\frac{1}{2}}\right)^{+}\left(b_{j1} - A_{j1}M_{j1}^{-1}Q_{j1}\right) \\ &=: \hat{Q}_{j1}\left(q_{j1}, \dot{q}_{j1}, t\right), \end{aligned} \tag{33}$$

where $M_{j1} \in n_{j1} \times n_{j1}$, $M_{j1} = diag[M_{j0}]$, composed of related basic unit quality matrix of M_{j0}, $Q_{j1} \in n_{j1} \times 1$, composed of related basic units Q_{j0} stacked together, Q_{j1}^{e} is n_{j1}-dimensional constraint torque matrix.

Next, based on establishing the dynamic models of each first-level subsystem, k_2 second-level subsystems will be formed by the constraint relationships between each subsystem, which can be expressed as:

$$A_{j2}(q_{j2}, \dot{q}_{j2}, t)\ddot{q}_{j2} = b_{j2}(q_{j2}, \dot{q}_{j2}, t), \tag{34}$$

where $j = 1, 2, \ldots k_1$, A_{j2} expresses the constraint matrix of $m_{j2} \times n_{j2}$, b_{j2} is m_{j2}-dimensional vector, q_{j2} is an n_{j2}-dimensional state vector, formed by the aggregation of state variables from each first-level nested subsystem within its second-level nested subsystems.

The motion equation of the second-level subsystem, derived from the constraint relationships in Equation (34), is described as follows:

$$\begin{aligned} M_{j2}\left(q_{j2}, t\right)\ddot{q}_{j2} &= Q_{j2}\left(q_{j2}, \dot{q}_{j2}, t\right) + Q_{j2}^{e}\left(q_{j2}, \dot{q}_{j2}, t\right) \\ &= Q_{j2}\left(q_{j2}, \dot{q}_{j2}, t\right) + M_{j2}^{\frac{1}{2}}\left(A_{j2}M_{j2}^{-\frac{1}{2}}\right)^{+}\left(b_{j2} - A_{j2}M_{j2}^{-1}Q_{j2}\right) \\ &=: \hat{Q}_{j2}\left(q_{j2}, \dot{q}_{j2}, t\right), \end{aligned} \tag{35}$$

where $M_{j2} \in n_{j2} \times n_{j2}$, $M_{j2} = diag[M_{j1}]$, composed of related basic unit quality matrix of M_{j1}, $Q_{j2} \in n_{j2} \times 1$, composed of related basic units Q_{j1} stacked together, Q_{j2}^{e} is n_{j2}-dimensional constraint torque matrix.

Similarly, if additional constraint relationships exist, the process can persist until the final tier of k_s s-level nested subsystems. Eventually, as shown in Figure 1, through the constraint relationships among the subsystems, the ultimate multi-body dynamics model is obtained.

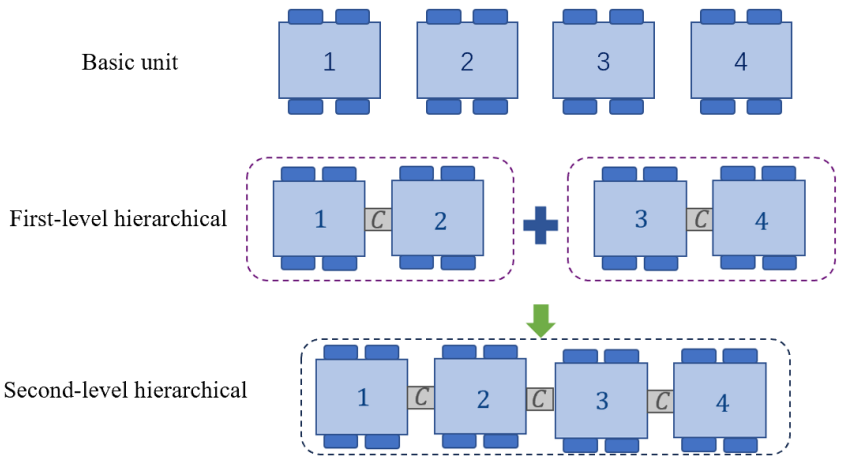


Figure 1. Schematic diagram of hierarchical modeling.

5. Hierarchical Dynamic Model of the Mobile Robots

This section applies the dynamic modeling method based on hierarchical constraint design mentioned above, and uses a fleet of four mobile robots as an example to demonstrate the above method. As shown in Figure 2, require the entire fleet to travel along a circle with a radius of $R = 10$ meters, and set the centroid distance between each mobile robot to $L = 1$ meter. The entire system consists of four basic units (mobile robots), with every two basic units forming a first-level hierarchical model. Finally, two first-level hierarchical models form a second-level hierarchical model.

Firstly, establish the dynamic models of each basic unit, using the four-wheel mobile robot dynamic model established by Li et al. [14], and arranged into the following matrix form. Table 1 lists the definitions of variables and parameters of the robot.

$$M_1\ddot{q} - Q_1(q, \dot{q}, t) = D_1(q, \dot{q}, t)\tau_1(t) \tag{36}$$

where

$$\begin{aligned} M_1 &= diag(m, m, I_z), q_1 = \begin{bmatrix} x & y & \varphi \end{bmatrix}^T \\ Q_1 &= -\begin{bmatrix} f_w\cos(\varphi) + f_{2v}\sin(\varphi) + f_{2z}r\cos(\varphi) - f_{1u}\cos(\varphi) \\ +C_f\frac{v+\dot{\varphi}a}{u}\sin(\varphi) \\ f_w\sin(\varphi) - f_{1u}\sin(\varphi) - C_f\frac{v+\dot{\varphi}a}{u}\cos(\varphi) \\ +f_{2z}r\sin(\varphi) - f_{2v}\cos(\varphi) \\ -C_f\frac{v+\dot{\varphi}a}{u}a + f_{2v}b \end{bmatrix} \\ D_1 &= \begin{bmatrix} -f_{1u}\sin(\varphi) + C_f\sin(\varphi) - C_f\frac{v+\varphi a}{u}\cos(\varphi) & \cos(\varphi) \\ f_{1u} - C_f\cos(\varphi) - C_f\frac{v+\dot{\varphi}a}{u}\sin(\varphi) & \sin(\varphi) \\ (f_{1u}a - C_f a) & 0 \end{bmatrix} \\ \tau_1 &= \begin{bmatrix} \delta \\ F_{drive} \end{bmatrix} \end{aligned} \tag{37}$$

Table 1. The symbol definitions of the mobile robot variables and parameters.

f_w	The air resistance
a	The distance from the center of gravity (CoG) to the front axle
b	The distance from the center of gravity (CoG) to the rear axle
C_f	The cornering stiffness of the front tire
u	The longitudinal velocity of the vehicle
v	The lateral velocity of the vehicle
r	The rolling resistance coefficient
$\dot{\varphi}$	The yaw rate of the vehicle
$f_{iv}\ (i = 1, 2)$	The lateral force of the front or rear tire
$f_{iu}\ (i = 1, 2)$	The longitudinal force of the front or rear tire
$f_{iz}\ (i = 1, 2)$	The vertical force of the front and rear tires
F_{drive}	The input drive/brake force

Secondly, the new unit is connected head-to-head with Unit 1, forming a four-axle vehicle configuration. When splicing, the geometric constraints between the two units are used as relative constraints to design the configuration. The geometric constraints between the units consist of two parts, with the first part being the relative position constraint:

$$(x_1 - x_2)^2 + (y_1 - y_2)^2 = L^2. \tag{38}$$

In this equation, L denotes the wheelbase of the unit. Take the second derivative of the position constraint with respect to time and express it in the form of $A_{12}\ddot{q}_{12} = b_{12}$, where

$$A_{12} = \begin{bmatrix} (x_1 - x_2) & (y_1 - y_2) & 0 & (x_2 - x_1) & (y_2 - y_1) & 0 \end{bmatrix}, \tag{39}$$

$$\ddot{q}_{12} = \begin{bmatrix} \ddot{x}_1 \\ \ddot{y}_1 \\ \ddot{\varphi}_1 \\ \ddot{x}_2 \\ \ddot{y}_2 \\ \ddot{\varphi}_2 \end{bmatrix}, b_{12} = \begin{bmatrix} -(\dot{x}_1 - \dot{x}_2)^2 - (\dot{y}_1 - \dot{y}_2)^2 \end{bmatrix}. \tag{40}$$

The dynamic equation for the vehicle configuration, formed by head-to-tail connection of two units, is:

$$M_{12}\ddot{q}_{12} = \hat{Q}_{12}, \tag{41}$$

$$\hat{Q}_{12} = Q_{12} + M_{12}^{\frac{1}{2}} \left(A_{12} M_{12}^{-\frac{1}{2}} \right)^{+} \left(b_{12} - A_{12} M_{12}^{-1} Q_{12} \right). \tag{42}$$

where

$$M_{12} = \begin{bmatrix} M_1 & 0 \\ 0 & M_1 \end{bmatrix} Q_{12} = \begin{bmatrix} \widetilde{Q}_{12} \\ Q_1 \end{bmatrix}, \tag{43}$$

$\widetilde{Q}_1$ represents the constraint force under servo constraints after applying the trajectory tracking task to the initial unit body.

Thirdly, the new unit is connected to the front and rear ends of the two-unit vehicle to form a six-axle vehicle configuration. During splicing, use the geometric constraints between the two units as relative constraints to design the configuration. The constraint of relative position is:

$$(x_1 - x_2)^2 + (y_1 - y_2)^2 = L^2, \tag{44}$$

$$(x_2 - x_3)^2 + (y_2 - y_3)^2 = L^2, \tag{45}$$

Take the second derivative of the position constraint with respect to time, and express it in the form of $A_{13}\ddot{q}_{13} = b_{13}$, where

$$A_{13} = \begin{bmatrix} (x_1 - x_2) & (y_1 - y_2) & 0 & (x_2 - x_1) & (y_2 - y_1) & 0 & 0 & 0 & 0 \\ 0 & 0 & 0 & (x_2 - x_3) & (y_2 - y_3) & 0 & (x_2 - x_3) & (y_2 - y_3) & 0 \end{bmatrix}, \tag{46}$$

$$\ddot{q}_{13} = \begin{bmatrix} \ddot{x}_1 \\ \ddot{y}_1 \\ \ddot{\varphi}_1 \\ \ddot{x}_2 \\ \ddot{y}_2 \\ \ddot{\varphi}_2 \\ \ddot{x}_3 \\ \ddot{y}_3 \\ \ddot{\varphi}_3 \end{bmatrix}, b_{13} = \begin{bmatrix} -(\dot{x}_1 - \dot{x}_2)^2 - (\dot{y}_1 - \dot{y}_2)^2 \\ -(\dot{x}_2 - \dot{x}_3)^2 - (\dot{y}_2 - \dot{y}_3)^2 \end{bmatrix}. \tag{47}$$

The dynamic equation for the entire vehicle configuration formed by connecting three units head-to-tail is:

$$M_{13}\ddot{q}_{13} = \hat{Q}_{13}, \tag{48}$$

$$\hat{Q}_{13} = Q_{13} + M_{13}^{\frac{1}{2}} \left(A_{13} M_{13}^{-\frac{1}{2}} \right)^{+} \left(b_{13} - A_{13} M_{13}^{-1} Q_{13} \right). \tag{49}$$

where

$$M_{13} = \begin{bmatrix} M_1 & 0 & 0 \\ 0 & M_1 & 0 \\ 0 & 0 & M_1 \end{bmatrix} Q_{13} = \begin{bmatrix} \widetilde{Q}_{13} \\ Q_1 \end{bmatrix}. \tag{50}$$

Finally, by sequentially assembling n modular units layer by layer, a two-axle complete vehicle configuration can be obtained. The constraint of relative position is:

$$(x_1 - x_2)^2 + (y_1 - y_2)^2 = L^2, \tag{51}$$

$$(x_2 - x_3)^2 + (y_2 - y_3)^2 = L^2, \tag{52}$$

$$\vdots$$

$$(x_{n-1} - x_n)^2 + (y_{n-1} - y_n)^2 = L^2, \tag{53}$$

Take the second derivative of the position constraint with respect to time, and express it in the form of $A_{1n}\ddot{q}_{1n} = b_{1n}$, where

$$A_{1n} = \begin{bmatrix} (x_1 - x_2) & (y_1 - y_2) & 0 & (x_2 - x_1) & (y_2 - y_1) & 0 \cdots \\ \vdots & & & & & \\ 0 \cdots & (x_{n-1} - x_n) & (y_{n-1} - y_n) & 0 & (x_{n-1} - x_n) & (y_{n-1} - y_n) \quad 0 \end{bmatrix}_{(n-1)\times 3n}, \tag{54}$$

$$\ddot{q}_{1n} = \begin{bmatrix} \ddot{x}_1 \\ \ddot{y}_1 \\ \ddot{\varphi}_1 \\ \ddot{x}_2 \\ \ddot{y}_2 \\ \ddot{\varphi}_2 \\ \cdots \\ \ddot{x}_n \\ \ddot{y}_n \\ \ddot{\varphi}_n \end{bmatrix}_{3n\times 1}, b_{1n} = \begin{bmatrix} -(\dot{x}_1 - \dot{x}_2)^2 - (\dot{y}_1 - \dot{y}_2)^2 \\ \vdots \\ -(\dot{x}_{n-1} - \dot{x}_n)^2 - (\dot{y}_{n-1} - \dot{y}_n)^2 \end{bmatrix}_{(n-1)\times 1}. \tag{55}$$

The dynamic equation for the entire vehicle configuration formed by connecting n units head-to-tail is:

$$M_{1n}\ddot{q}_{1n} = \hat{Q}_{1n}, \tag{56}$$

$$\hat{Q}_{1n} = Q_{1n} + M_{1n}^{\frac{1}{2}}\left(A_{1n}M_{1n}^{-\frac{1}{2}}\right)^{+}\left(b_{1n} - A_{1n}M_{1n}^{-1}Q_{1n}\right). \tag{57}$$

where

$$M_{1n} = \begin{bmatrix} M_1 & 0 & 0 & 0 & 0 \\ 0 & M_1 & 0 & 0 & 0 \\ 0 & 0 & \ddots & 0 & 0 \\ 0 & 0 & 0 & 0 & M_1 \end{bmatrix}_{n\times n} Q_{1n} = \begin{bmatrix} \widetilde{Q}_{1n} \\ Q_1 \end{bmatrix}. \tag{58}$$

In general, this section constructs a modular unit-scalable dynamic analytical model. According to the coupling characteristics among modules, the kinematic constraints of the vehicle are integrated into the dynamic models of each modular unit, leading to a nested extended hierarchical constraint dynamic modeling approach in analytical form. The hierarchical nested modeling process is exemplified in Figure 2. The analytical model of a modular unit is easy to obtain, and in full-vehicle modeling, unit analytical models can be rapidly combined using hierarchical nested constraints to derive the analytical dynamic model of two-unit assemblies. Similarly, the unit models are continuously combined until

the modeling of the complete vehicle with n units is achieved. This multi-module hierarchical nested analytical modeling approach streamlines the modeling process, improves the generality and applicability of the model, and offers an effective method for scalable vehicle configuration modeling. [15]

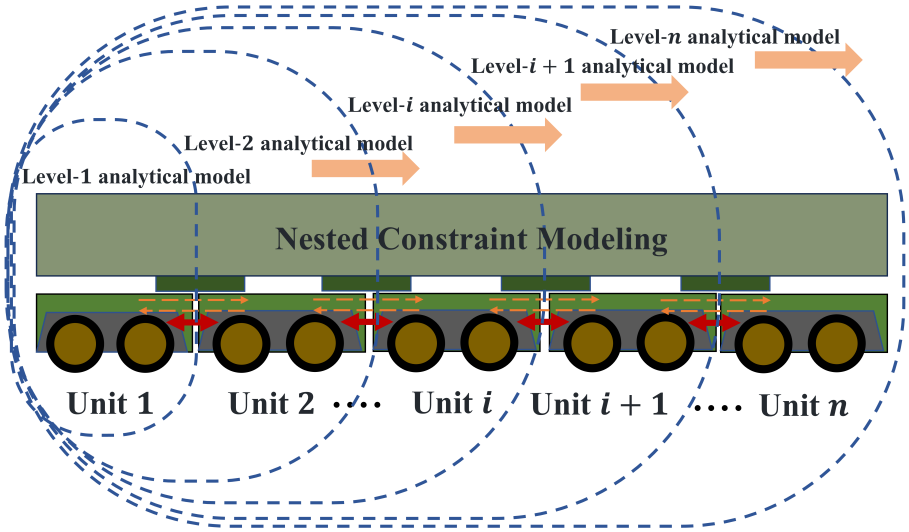


Figure 2. Diagram of the hierarchical nested constraint modeling process for multiple modules.

6. Controller Scheme

Consider the following mechanical system:

$$M(q(t),t)\ddot{q}(t) + C(q(t),\dot{q}(t),t)\dot{q}(t) + g(q(t),t) = B(q(t),\dot{q}(t),t)\tau(t), \tag{59}$$

where $\tau \in \mathbb{R}^m$ is the control input vector, C is the Coriolis/centrifugal force, $g(q,\dot{q},t)$ is the gravitational force, and the input matrix $B(q,\dot{q},t)$, each of which possesses dimensions deemed appropriate. The functions $C(\cdot)$, $g(\cdot)$, and $B(\cdot)$ are posited to maintain continuity. It can be chosen by the designer for convenience based on the specifications of the problem. Specifically, the system (59) includes both fully actuated (when $m = n$) and underactuated (when $m < n$) systems.

Let $\ddot{m}_q := M^{\frac{1}{2}}\ddot{q}$, $n := M^{-\frac{1}{2}}(-C\dot{q} - g)$, and $\tau := \tau_q$; then, the system (59) can be reformulated as follows:

$$\ddot{m}_q = n + M^{-\frac{1}{2}}B\tau_q, \tag{60}$$

and the constraint (3) can be revised as follows:

$$\Xi_1\ddot{m}_q = b, \tag{61}$$

with $\Xi_1(q,t) = AM^{-\frac{1}{2}}$.

The constraint (61) is consistent if, for a given Ξ_1 and b, there is at least one solution, $\ddot{m}_q$.

Since there is a one-to-one correspondence between $\ddot{m}_q$ and $\ddot{q}$.

Let $\tilde{b} := b - \Xi_1 n$, $\Xi_2 := M^{-\frac{1}{2}}B$, with (60) and (61); we can obtain:

$$(\Xi_1\Xi_2)\tau_q = \tilde{b}, \tag{62}$$

where $\tau_q \in \mathbb{R}^m$ represents the unknown force; this equation serves as a constraint on τ_q. The controllability of constraint dynamic system (59) with $A\ddot{q} = b$ necessitates the consistency of (62).

Equation (62) is consistent: if, for a given $(\Xi_1\Xi_2)$ and $\tilde{b}$, there is at least one solution, τ_q.

For the general underactuated dynamic constraint system (59), the following theoretical results are obtained:

$$\tau_q(q,\dot{q},t) = (\Xi_1\Xi_2)^+\tilde{b} + \left[I - (\Xi_1\Xi_2)^+(\Xi_1\Xi_2)\right]S, \tag{63}$$

where $S \in \mathbb{R}^m$ represents an arbitrary vector, potentially dependent on q, t. Additionally, consider inequality constraints.

The constraint control quantity τ_q ensures the satisfaction of the equality constraint (3). However, the presence of an initial error means that relying solely on the constraint control quantity τ_q is insufficient for the system to meet these constraints. In practice, satisfying these constraints at the initial moment is often challenging due to a variety of factors. Therefore, introducing a control quantity capable of addressing the initial error is essential.

Let $E(q,\dot{q},t) := M^{-1}(q,\dot{q},t)$, and

$$\rho(q,\dot{q},t) := A(q,\dot{q},t)\dot{q} - c(q,\dot{q},t), \tag{64}$$

$$\hat{\rho}(q,\dot{q},t) := [PA(q,\dot{q},t)E(q,\dot{q},t)B(q,\dot{q},t)]^T\rho(q,\dot{q},t), \tag{65}$$

where $P \in \mathbb{R}^{m\times m}$ is an arbitrary symmetric positive definite matrix, and $c \in \mathbb{R}^{m\times 1}$ represents an m-dimensional vector.

There exists a known constant, $\underline{\lambda} > 0$, for all $q \in \mathbb{R}^n$, $\dot{q} \in \mathbb{R}^n$, $t \in \mathbb{R}$, such that $\lambda_m\left[(PAEB)\times(PAEB)^T\right] \geq \underline{\lambda}$, where $\lambda_m(\cdot)$ represents the minimum eigenvalue of the matrix in the parentheses.

To address potential deviations in initial conditions, the following controls are proposed:

$$\tau_p(q,\dot{q},t) = -\kappa\hat{\rho}(q,\dot{q},t), \tag{66}$$

where $\kappa > 0$ is a constant.

The final control design for system (59) is proposed as follows: [16]

$$\tau = \tau_q(q,\dot{q},t) + \tau_p(q,\dot{q},t). \tag{67}$$

Theorem 2. *Consider the system* (59)*; the control* (67) *renders the following performance:*
(i) Uniform stability: For each $\beta > 0$, there exists $\delta > 0$, such that, if $\rho(\cdot)$ is any solution with $\|\rho(t_0)\| < \delta$, then $\|\rho(t)\| < \beta$, for all $t > t_0$.
(ii) Converge to zero: For a given constraint (61)*,*

$$\lim_{t\to\infty}\rho = 0. \tag{68}$$

Proof of Theorem 2. Choose the Lyapunov function candidate as:

$$\bar{V} = \rho^T P\rho, \tag{69}$$

.

In the proof, for simplicity, arguments of functions are omitted when confusion is unlikely. Taking the derivative of $\bar{V}$ with respect to t yields:

$$\begin{aligned}\dot{\hat{V}} &= 2\rho^T P\dot{\rho} \\ &= 2\rho^T P(A\ddot{q} - b) \\ &= 2\rho^T P\Big\{A\Big[M^{-1}(-C\dot{q} - g) + M^{-1}B(\tau_q + \tau_p)\Big] - b\Big\} \\ &= 2\rho^T P\Big[AM^{-1}(-C\dot{q} - g) + AM^{-1}B\tau_q - b\Big] \\ &+ 2\rho^T PAM^{-1}B\tau_p.\end{aligned} \tag{70}$$

Note that $AM^{-1}(-C\dot{q} - g) = \Xi_1 n$, $AM^{-1}B = \Xi_1\Xi_2$. Equation (63) yields:

$$\begin{aligned}&AM^{-1}(-C\dot{q} - g) + AM^{-1}B\tau_q - b \\ &= \Xi_1 n + \Xi_1\Xi_2\tau_q - b \\ &= \Xi_1 n + b - \Xi_1 n - b \\ &= 0.\end{aligned} \tag{71}$$

According to Rayleigh's principle, we have

$$\begin{aligned}2\rho^T PAM^{-1}B\tau_p &= -2\kappa\rho^T PAEB(PAEB)^T\rho \\ &\leq -2\kappa\lambda_m\Big(PAEB(PAEB)^T\Big)\|\rho\|^2 \\ &\leq -2\overline{\kappa}\|\rho\|^2,\end{aligned} \tag{72}$$

where $\overline{\kappa}$ denotes the $\kappa\underline{\lambda}$.

Combining (70)-(72), we can obtain

$$\dot{\hat{V}} \leq 0 - 2\overline{\kappa}\|\rho\|^2 = -2\overline{\kappa}\|\rho\|^2. \tag{73}$$

From (73), given that the upper bound of the derivative of $\bar{V}$ is nonpositive and equals zero if and only if $\rho = 0$, it follows that there is uniform stability and convergence of ρ to 0 as $t \to \infty$. □

7. Numerical Simulations

This section takes the transportation system composed of four miniature modular robots as an example and elaborates the numerical simulation of the reconfigurable miniature modular robotic swarm. It aims to verify the effectiveness of the proposed unified modeling and coordination control strategy for the reconfigurable micro-robotic transport platform. The circular reference trajectory with radius $R = 10$ m is adopted for the swarm system, and key initial simulation parameters are listed in Table 2.

When the unit receives a trajectory tracking task, it treats the trajectory to be tracked as a constraint. Take the second derivative of the position constraint with respect to time, and express it in the form of $A_1\ddot{q}_1 = b_1$. Taking a circular constraint trajectory as an example:

$$x_1 = 10\sin t, y_1 = -10\cos t, \tag{74}$$

$$x_1^2 + y_1^2 = 10^2, \tag{75}$$

where

$$A_1 = \begin{bmatrix}x_1 & y_1 & 0\end{bmatrix}, b_1 = \begin{bmatrix}-\dot{x}_1^2 - \dot{y}_1^2\end{bmatrix}. \tag{76}$$

Under the trajectory constraint, the dynamics equation of the unit changes to [17–20]:

$$M_1\ddot{q}_1 = \widetilde{Q}_1, \tag{77}$$

where

$$\widetilde{Q}_1 = Q_1 + Q_1^c, \tag{78}$$

$$Q_1^c = M_1^{\frac{1}{2}}\left(A_1 M_1^{-\frac{1}{2}}\right)^+\left(b_1 - A_1 M_1^{-1} Q_1\right). \tag{79}$$

Table 2. Initial condition.

Parameter	Value	Parameter	Value
x_1	10.5000 m	x_2	10.4500 m
y_1	−0.5000 m	y_2	−1.4987 m
φ_1	1.5708 rad	φ_2	1.4708 rad
$\dot{x}_1$	0 m/s	$\dot{x}_2$	0.9987 m/s
$\dot{y}_1$	10 m/s	$\dot{y}_2$	9.9500 m/s
$\dot{\varphi}_1$	1 rad/s	$\dot{\varphi}_2$	1 rad/s
x_3	10.3005 m	x_4	10.0530 m
y_3	−2.4875 m	y_4	−3.4564 m
φ_3	1.3707 rad	φ_4	1.2707 rad
$\dot{x}_3$	1.9875 m/s	$\dot{x}_4$	2.9564 m/s
$\dot{y}_3$	9.8005 m/s	$\dot{y}_4$	9.5530 m/s
$\dot{\varphi}_3$	1 rad/s	$\dot{\varphi}_4$	1 rad/s

To facilitate the reproduction of the numerical experiments and make the simulation setup self-contained, Tables 3 and 4 summarize the key simulation parameters. Table 3 lists the physical parameters of each modular vehicle unit, including the mass, yaw moment of inertia, air drag coefficient, front and rear tire cornering stiffnesses, rolling resistance coefficient, distances from the center of gravity to the front and rear axles, and gravitational acceleration. Table 4 provides the controller and numerical simulation settings, including the damping gain, positive definite matrix P, null-space vector S, minimum longitudinal velocity threshold, simulation step size, ODE solver, integration tolerances, pseudoinverse rank tolerance, and controller sampling interval.

Table 3. Parameters of vehicle model.

Parameter	Value
Mass m	1.5 kg
Yaw Inertia Moment I_z	0.0042 kg · m^2
Air Drag Coefficient c_x	0.0021 m^2
Front tire cornering stiffness C_f	−18 N/°
Rear tire cornering stiffness C_r	−18 N/°
Rolling resistance coefficient r	0.012
Distance from CoG to front axle a	0.075 m
Distance from CoG to rear axle b	0.065 m
Gravity acceleration g	9.8 m/s^2

The three-dimensional trajectory-versus-time evolution of four serially connected miniature modular robots is illustrated in Figure 3. Each colored curve represents the time-history spatial trajectory of an individual robot module. It can be observed that all modules start from non-ideal initial states with pose deviations and gradually converge toward the desired circular reference trajectory as the control loop proceeds.

Table 4. Controller and numerical simulation parameters.

Parameter	Value
Damping gain κ	5
Positive definite matrix P	$\mathrm{diag}([1,1,1])$
Null-space vector S	0
Minimum longitudinal velocity $u_{\min}$	0.05 m/s
Simulation step size	0.001 s
ODE solver	ODE15s
Relative integration tolerance	10^{-7}
Absolute integration tolerance	10^{-8}
Moore–Penrose pseudoinverse rank tolerance	10^{-10}
Controller sampling interval	0.001 s

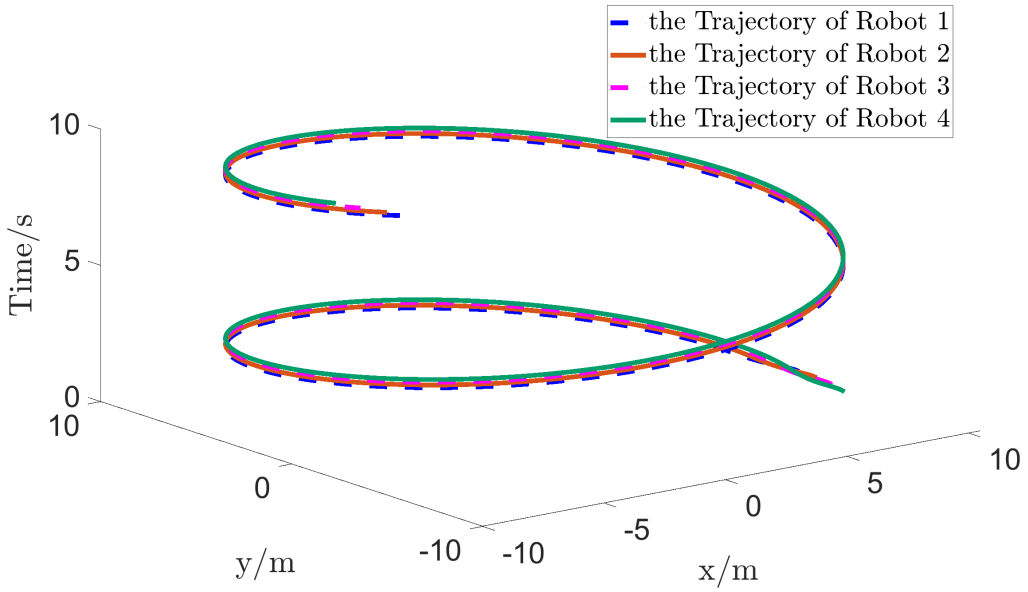


Figure 3. Three-dimensional time-history trajectories of four serially connected modular robots. All modules converge from deviated initial poses to the target circular reference trajectory under the nested constraint following control.

Figure 4 presents the spatial trajectory comparison for four miniature modular robots in a 3-D waterfall layout. Each robot moves along its circular orbit at different Y-axis layers corresponding to robot indices. Owing to inter-module geometric constraints, the circular trajectories of the four modules maintain consistent motion characteristics, which reflects the coordinated kinematic performance of the serial-connected swarm system.

Figure 5a–d shows the time-domain responses of front-wheel steering angles for the four modules. An external torque disturbance with an amplitude of 1 N · m is imposed on the system within $t = 4$ s to $t = 6$ s to verify the disturbance-rejection capability of the proposed controller. Influenced by initial pose offsets, each robot exhibits an obvious front-wheel steering-angle deviation at $t = 0$. Under the hierarchical nested constraint-following control, the front-wheel steering-angle deviations decay quickly and stabilize near the ideal value, indicating that the steering-angle synchronization requirement among serially connected modules is well satisfied even under external perturbation. Figure 6a–d presents the driving torque responses of each miniature modular robot under the same 1 N · m torque disturbance from $t = 4$ s to $t = 6$ s. It can be observed that the driving torques produce moderate transient variations to counteract the external perturbation during the disturbance interval. After the disturbance disappears, the control torques rapidly return to their original steady-state levels without sustained oscillations, which demonstrates that

the hierarchical nested constraint-following control possesses favorable anti-disturbance performance for modular swarm robotic systems.

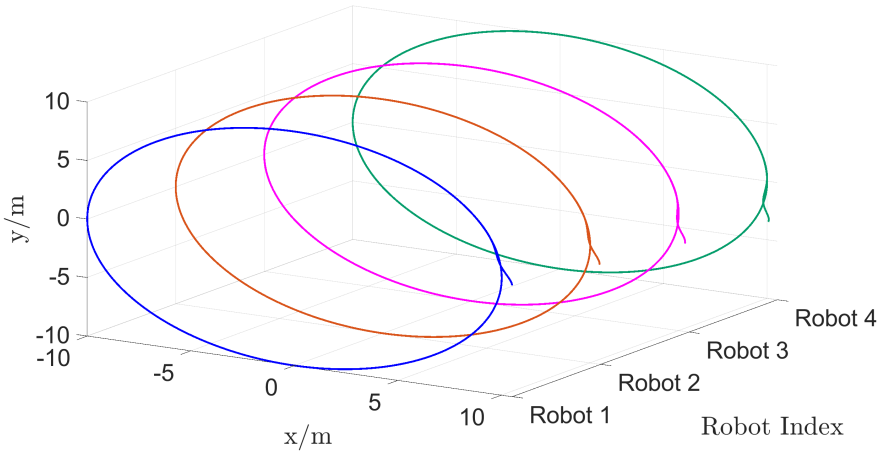


Figure 4. Comparison diagram of trajectories for four miniature modular robots. It demonstrates that the four modules maintain consistent circular motion characteristics subject to inter-module geometric constraints for swarm coordination.

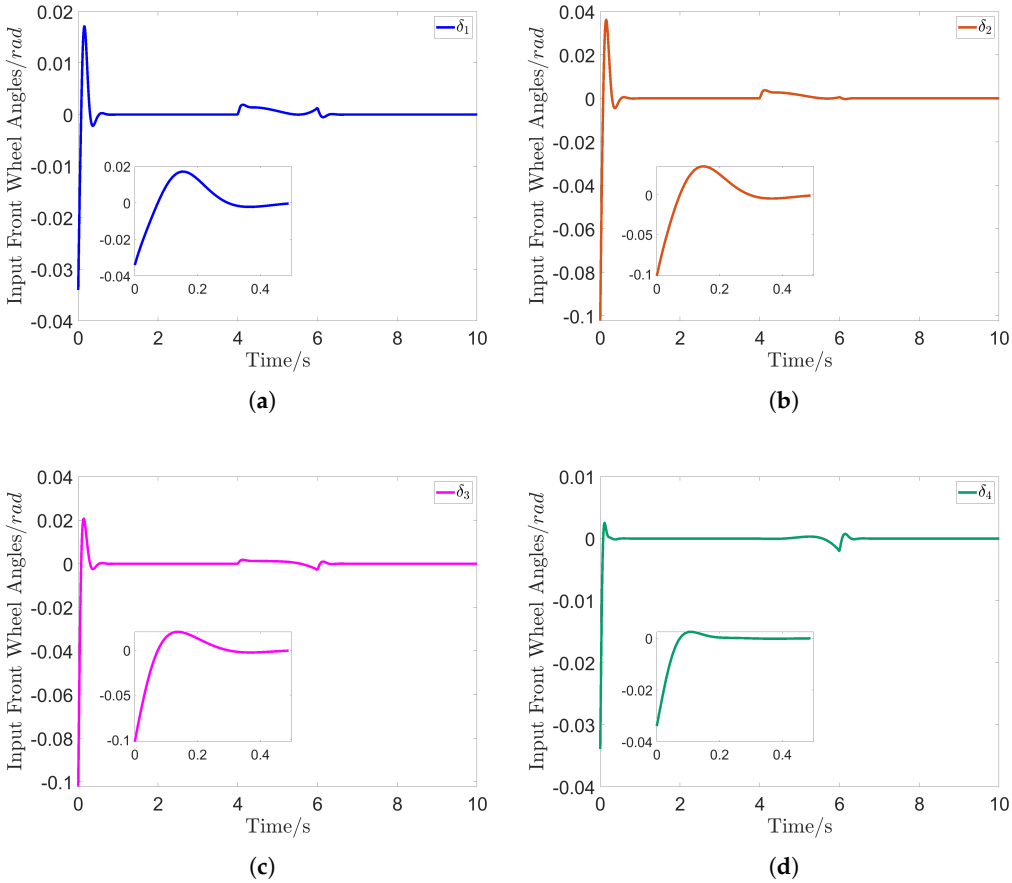


Figure 5. Front-wheel steering input of four miniature modular robots. (**a**) Front-wheel steering input of the first miniature modular robot. (**b**) Front-wheel steering input of the second miniature modular robot. (**c**) Front-wheel steering input of the third miniature modular robot. (**d**) Front-wheel steering input of the fourth miniature modular robot. It shows that under an external torque disturbance of amplitude 1 N · m applied from $t = 4$ s to $t = 6$ s, initially, the front wheel angle deviations decay rapidly and steering angle synchronization among serially connected modules is well maintained under the proposed control framework.

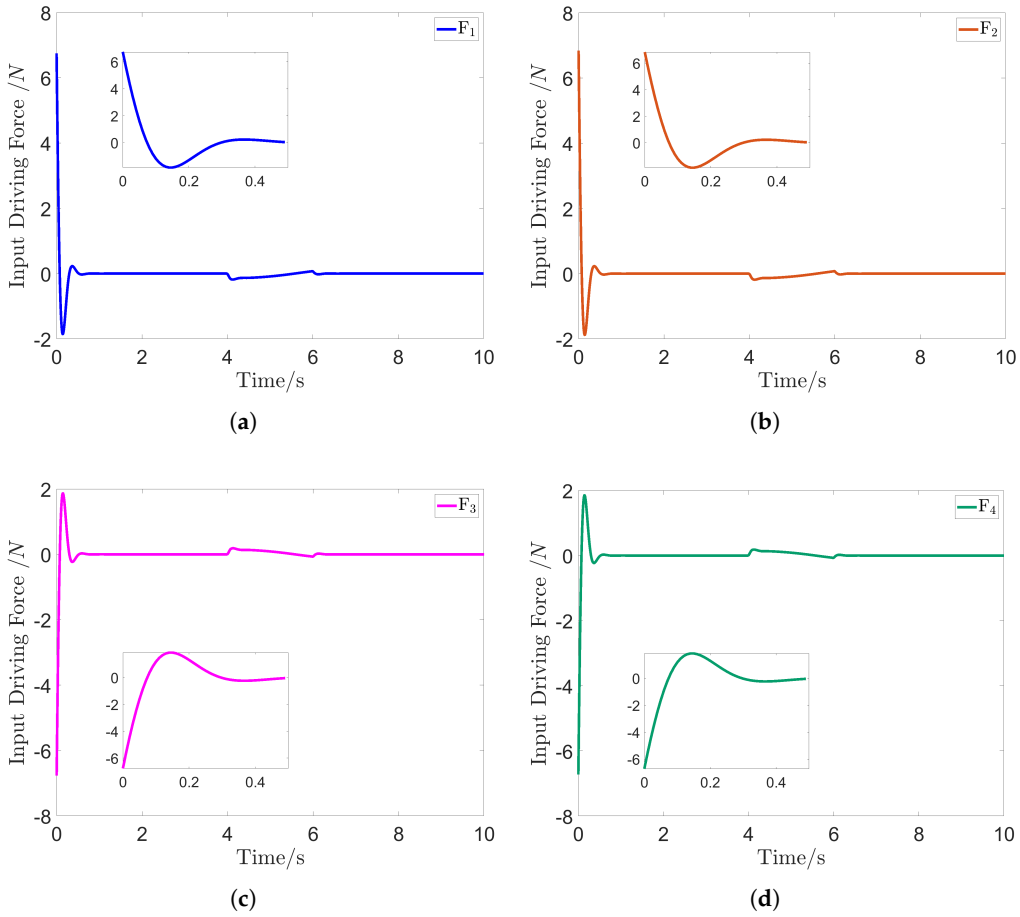


Figure 6. Driving torques of four miniature modular robots. (**a**) Driving torque of the first miniature modular robot. (**b**) Driving torque of the second miniature modular robot. (**c**) Driving torque of the third miniature modular robot. (**d**) Driving torque of the fourth miniature modular robot. It reveals that, when an external torque disturbance of amplitude 1 N · m is imposed on the system within $t = 4$ s to $t = 6$ s, control torques produce moderate transient responses against perturbation and quickly return to steady-state values after the disturbance disappears.

The velocity-magnitude spatial distribution surfaces of four miniature modular robots are given in Figure 7a–d. Each subplot contains the planar actual trajectory projected onto the X–Y plane and the corresponding 3-D velocity-magnitude surface above the trajectory. The color bar quantifies the magnitude of the module velocity at different spatial points. It can be seen that the velocity magnitude of each module remains relatively stable during circular tracking, which is consistent with the expected constant-speed circular transportation mission.

To further verify the generality of the proposed controller under complex trajectories and its anti-interference capability against parameter uncertainties, an additional simulation case with an eight-shaped reference trajectory and parameter perturbation is conducted.

The ideal eight-shaped reference trajectory contains continuous curvature variation and crossing points, presenting higher tracking difficulty than the circular trajectory. To test the anti-interference capability of the controller against parameter uncertainties, a 20% positive deviation is imposed on the mass parameter of Robot 2, simulating the payload variation or parameter mismatch in practical applications. The other three robots maintain nominal dynamic parameters, and all initial pose deviations are consistent with the circular trajectory simulation settings.

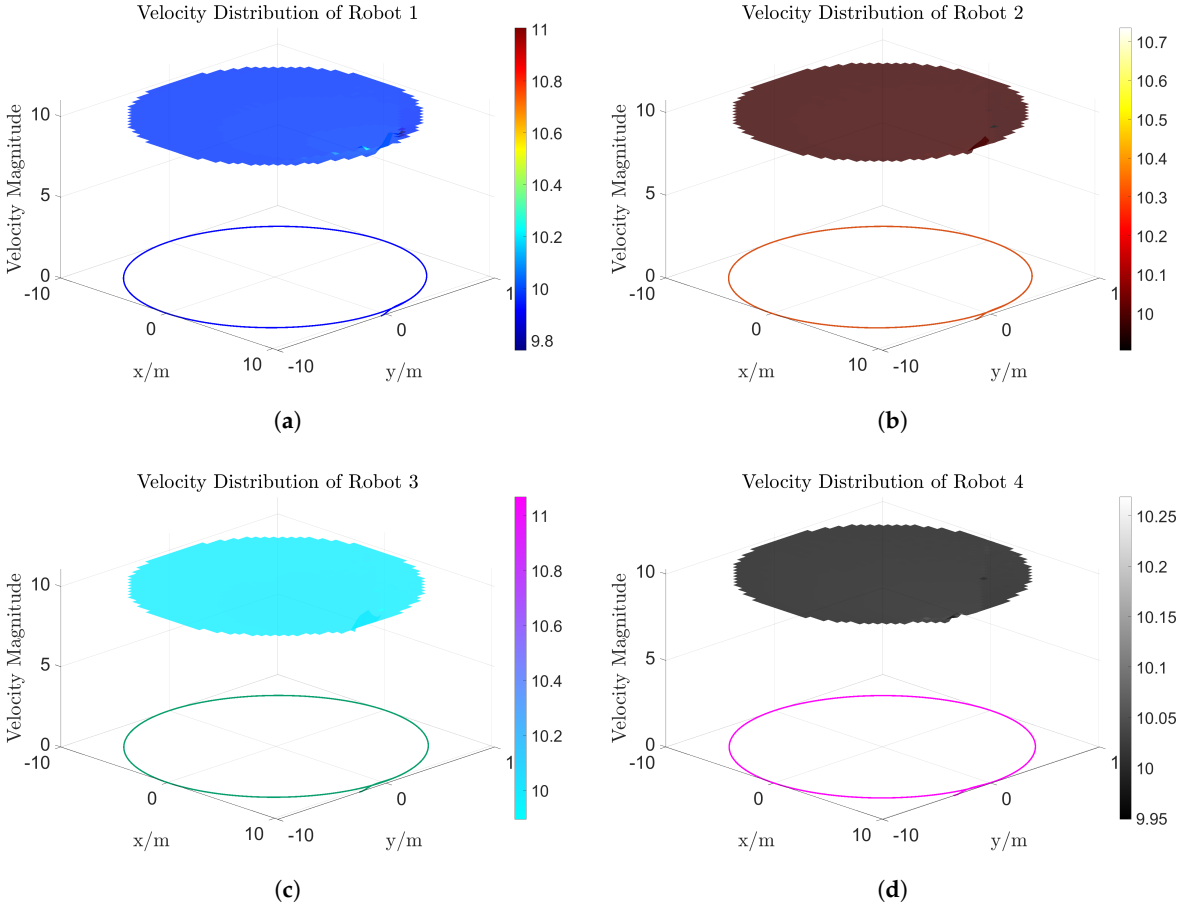


Figure 7. Velocity distribution surfaces of four miniature modular robots. (**a**) Velocity distribution surface of the first miniature modular robot. (**b**) Velocity distribution surface of the second miniature modular robot. (**c**) Velocity distribution surface of the third miniature modular robot. (**d**) Velocity distribution surface of the fourth miniature modular robot. It indicates that each robot maintains relatively stable velocity magnitude when performing the constant speed circular cooperative transportation mission.

The planar trajectory tracking results of the four modules under the 8-shaped trajectory are shown in Figure 8. It can be observed that all four robot modules converge to the ideal 8-shaped reference trajectory rapidly after the initial transient phase. Even with 20% mass parameter uncertainty, Robot 2 (orange curve) only exhibits minor tracking deviations at the positions with large curvature (the four arc vertices of the 8-shape), and still maintains close following of the reference trajectory throughout the whole motion process. No sustained divergence or oscillation occurs, which demonstrates that the proposed nested constraint-following controller possesses strong anti-interference capability against parameter perturbations, and can maintain stable tracking performance under complex curved trajectories and model mismatches.

Significant initial tracking deviations exist at the starting instant due to mismatched initial conditions. Benefiting from the embedded damping correction term within the constraint-following control law, the trajectory errors of all four miniature modular robots rapidly decay and converge toward zero within 0.5 s. Figure 9 presents the time-domain trajectory tracking error curves of each robot. It can be observed that both controllers converge to zero, while the proposed constraint-following controller achieves lower peak error and smaller steady-state tracking deviation compared with the LQR baseline, demonstrating better trajectory tracking performance for modular swarm transportation systems. After

convergence, minor residual errors remain, which can be attributed to numerical integration tolerances. Figure 10 shows the comparison of cumulative tracking error between the proposed controller and the LQR controller for four miniature modular robots, where the cumulative tracking error of LQR is significantly higher than that of the proposed method for all four vehicles. The simulation result demonstrates that the proposed cooperative control framework can effectively eliminate initial tracking errors for reconfigurable modular robot swarms.

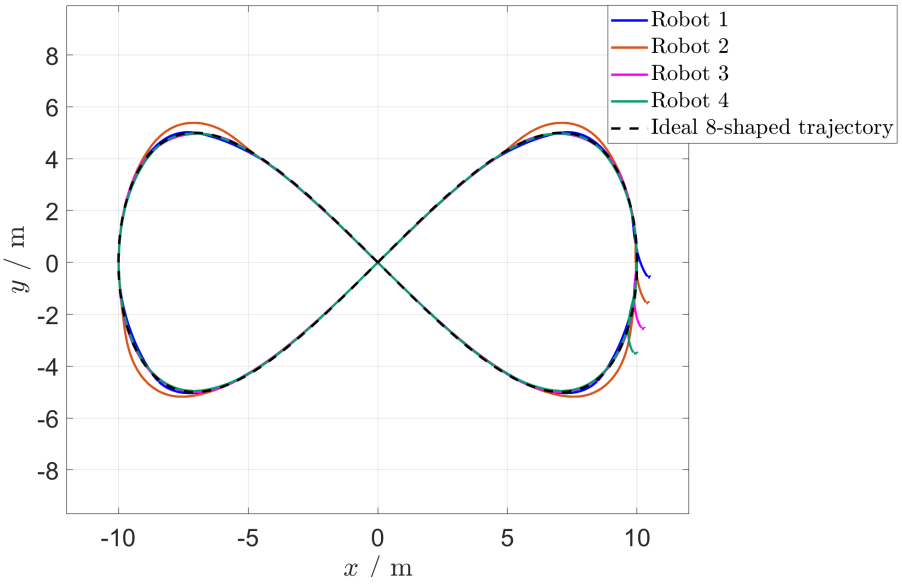


Figure 8. Trajectory tracking results of four serially connected modular robots under eight-shaped reference trajectory with 20% mass uncertainty on Robot 2.

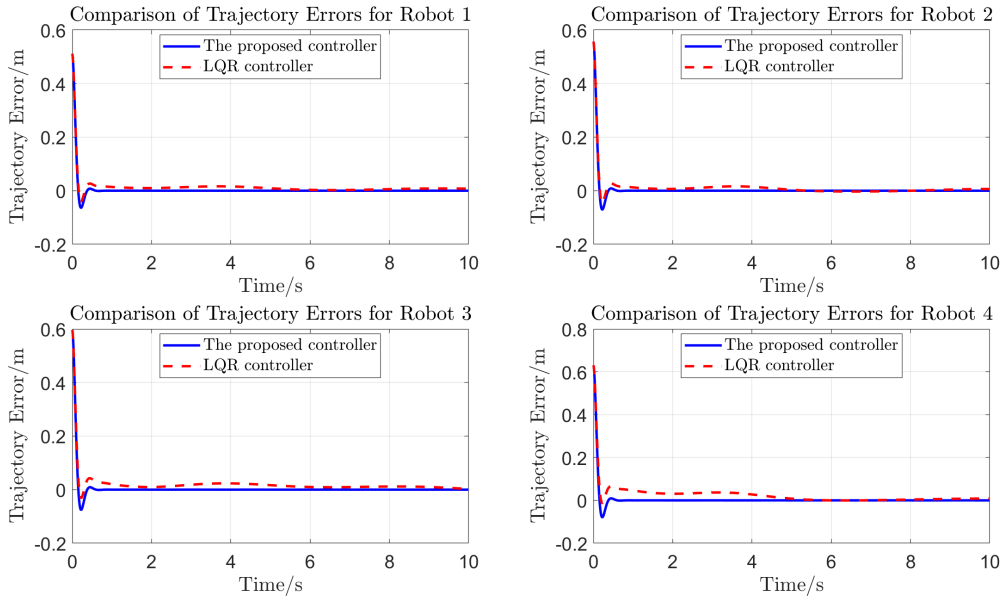


Figure 9. Comparison of trajectory errors between the proposed controller and LQR for four miniature modular robots. It shows that the nested constraint following controller yields lower peak error and smaller steady-state deviation than the LQR controller under identical initial conditions.

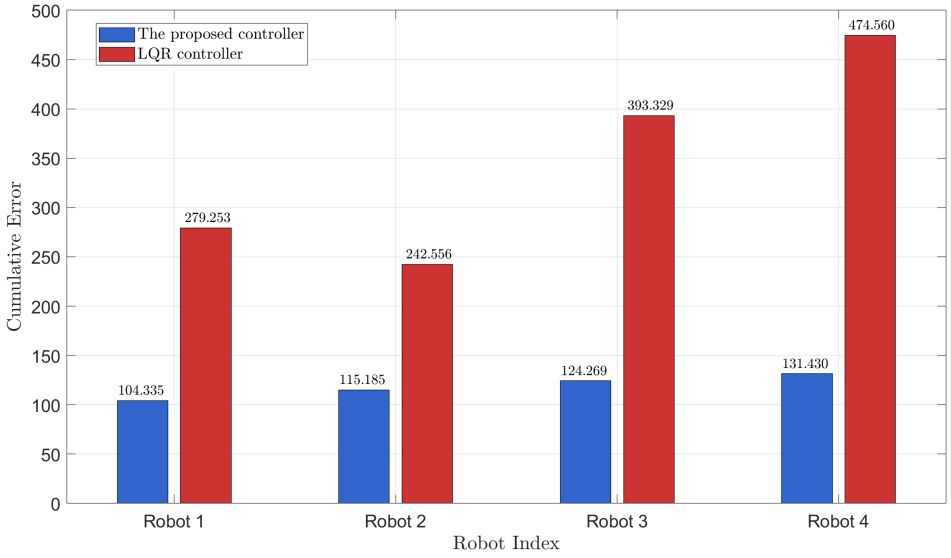


Figure 10. Cumulative error comparison between the proposed controller and LQR for four miniature modular robots. It demonstrates that the proposed cooperative control framework achieves considerably lower cumulative tracking error for every robot module compared with the LQR baseline approach.

Supplementary eight-module serial-swarm simulation results are illustrated in Figures 11 and 12. The eight-robot case shows that the proposed nested constraint-following framework can still enforce circular trajectory tracking and inter-module distance constraints as module quantity increases. Tracking errors for all eight modules converge toward near-zero within 0.5s, which is consistent with the four-module case.

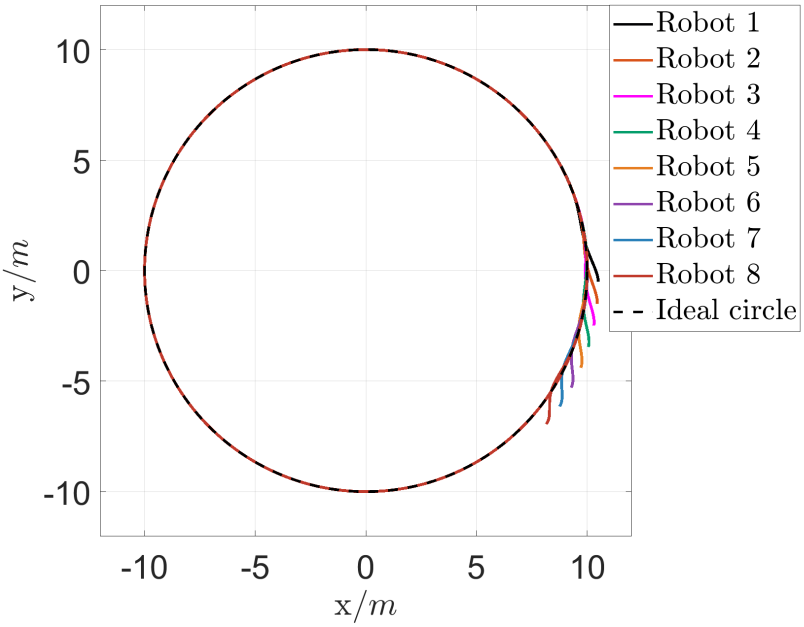


Figure 11. Collective planar trajectories of eight serially-connected miniature modular robots. All eight modules converge to the target circular reference orbit under nested constraint-following control.

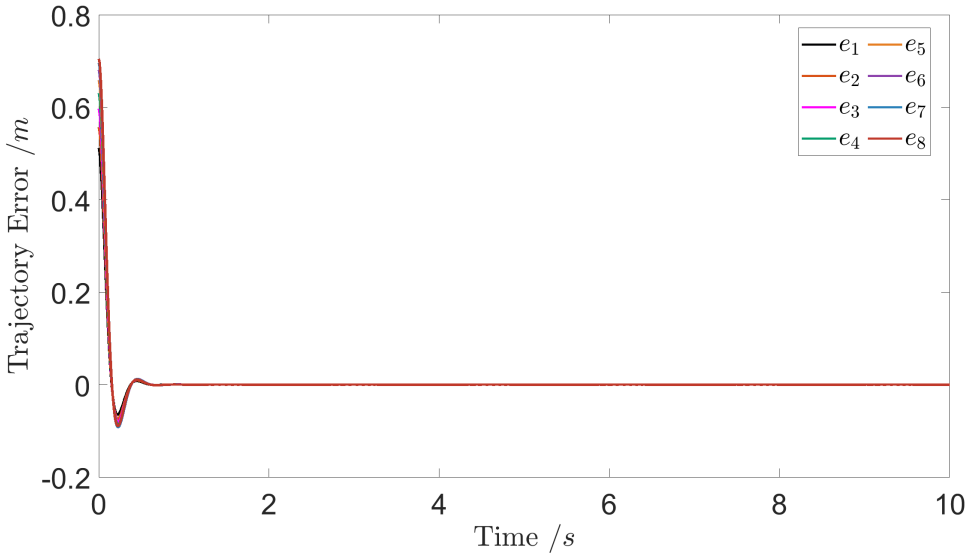


Figure 12. Radial trajectory-tracking errors of eight serially-connected miniature modular robots. The radial distance error of each module decays rapidly and converges close to zero.

To quantitatively substantiate the computational scalability of the proposed hierarchical nested modeling framework, we record the core dynamic computation runtime of four-module and eight-module serial swarm simulations under identical simulation settings. All simulations are executed on a desktop PC equipped with an Intel Core i7-12700H 2.7 GHz CPU and 16 GB of RAM, with a total simulation duration of 10 s and a fixed numerical integration step size of 0.001 s. The runtime statistics are summarized in Table 5.

Table 5. Core computation runtime of swarm systems with different module counts.

Module Quantity	Core Dynamic Computation Runtime (s)	Relative Growth Ratio
4	3.3034	1.00 (baseline)
8	10.7857	3.27

As shown in Table 5, when the number of modules doubles from four to eight, the total core computation runtime increases by a factor of 3.27. For conventional monolithic full-system modeling, the dimension of the generalized state vector grows linearly with module count, and the matrix pseudoinverse operation exhibits approximately quadratic computational complexity, which would lead to a roughly four-fold runtime growth when the module count doubles. The lower-than-quadratic runtime growth verifies that the hierarchical nested recursive structure effectively avoids the explosive growth of computational overhead brought by full matrix reconstruction, and provides favorable computational scalability for variable-scale modular swarm systems. This computational advantage makes the proposed framework more suitable for real-time embedded deployment on miniature modular robot units.

In summary, numerical simulations in this section systematically verify the trajectory-tracking accuracy, heading synchronization performance, and disturbance-rejection capability of the proposed hierarchical nested constraint-following modeling and control framework. Comparative tests with the LQR baseline controller demonstrate the superiority of the proposed method in both peak deviation and cumulative tracking error. The eight-shaped trajectory test with parameter perturbation further validates the anti-interference capability of the controller against parameter uncertainties under complex

paths and model mismatch. The supplementary eight-module simulation and runtime analysis quantitatively confirm the computational scalability of the recursive nested architecture. Nevertheless, full-system computational overhead grows as the number of modules increases. We leave systematic large-scale benchmark tests with dozens of units as a direction for our follow-up investigation to further quantify the computational efficiency and numerical stability of the presented recursive modeling framework.

8. Discussion

Although the numerical simulations demonstrate the effectiveness of the proposed hierarchical nested constraint-following framework, several practical implementation challenges remain to be addressed when deploying the algorithm onto real miniature modular robotic transportation swarms. We discuss key hardware-oriented challenges including computational burden, sensing demands, time synchronization, inter-module wireless communication, robustness against modeling mismatch, and hardware-oriented scalability.

First, regarding computational requirements. The nested recursive solution relies on Moore-Penrose generalized inverse operations. For embedded onboard microcontrollers of miniature robots, repeated matrix pseudoinverse brings non-negligible computational burden. The hierarchical recursive structure helps avoid assembling huge global matrices, yet onboard computation resources still impose upper limits on the maximum number of parallel modules that can be handled in real-time. As observed from the eight-module simulation case, the simulation runtime increases evidently with module count, which further illustrates this computational challenge for real-time embedded implementation.

Second, sensing requirements. Each modular unit needs accurate onboard sensing to obtain its pose, velocity, and relative position with adjacent connected modules. Real-world sensor noise, drift, and measurement bias will directly propagate into constraint equations. High-precision inertial measurement units combined with relative ranging sensors are required to provide reliable state information for constraint-following dynamic computation.

Third, inter-module time synchronization. Recursive nested modeling and cooperative control demand consistent time stamps across all connected robot modules. Clock drift among distributed embedded controllers will violate inter-module geometric acceleration constraints and introduce extra tracking errors. Precise time synchronization protocols are necessary to align the sampling and control update instants of each unit.

Fourth, wireless communication constraints. Distributed recursive computation requires limited information exchange between neighboring modules. Practical wireless links suffer from transmission delay, packet loss, and bandwidth limitation. Communication latency can degrade constraint satisfaction performance, which calls for delay-aware control adjustment for real hardware deployment.

Fifth, robustness to modeling errors. The derivation of UK constraint-following dynamics is built upon nominal dynamic parameters. In physical systems, uncertain mass, tire-ground friction variation, and unmodeled disturbance constitute model mismatch. Although the damping correction term in the control law suppresses initial tracking deviations, further robust control modification will be essential to cope with persistent model uncertainties in hardware experiments.

Finally, scalability on real hardware. The theoretical scalability derived from recursive modeling cannot be fully reproduced in practice. As the number of robot modules increases, cumulative sensing noise, communication overhead, and synchronization error will gradually degrade overall swarm performance. Hardware-level scalability is jointly restricted by onboard computing capacity, sensor accuracy, and communication reliability.

To bridge the gap between numerical simulation and physical deployment, our research group is currently constructing a miniature modular robot hardware testbed. Each modular unit adopts an integrated steering micro chassis with overall dimensions of 170 mm $\times$ 140 mm $\times$ 60 mm and a unit mass of approximately 1.5 kg. The physical prototype is designed as an underactuated system, which is fully consistent with the underactuated nonlinear dynamic model adopted in the numerical simulation. For onboard computation, each module is equipped with a 32-bit ARM Cortex-M7 embedded microcontroller with a main frequency of 480 MHz and 1 MB of on-chip SRAM, which is responsible for real-time dynamic solution, control law calculation and peripheral driving. For state perception, each unit integrates a six-axis MEMS inertial measurement unit (IMU) with $0.05^\circ/\mathrm{s}$ gyroscope bias for attitude and velocity estimation, and a 100 Hz optical flow sensor for planar position measurement. For inter-module relative perception, an infrared ranging module with ± 1 mm accuracy is installed at the front and rear of each chassis to obtain relative position deviations between connected units. For motion actuation, each module adopts a dual-wheel independent drive scheme with high-torque micro DC motors. For inter-module data interaction, a 2.4 GHz wireless communication protocol with a 1 ms communication period is adopted to support time synchronization and state information exchange between adjacent units.

Physical prototype validation is reserved for future work, as our high-fidelity miniature modular robot testbed is still under construction. The above practical challenges will serve as important guidelines when we port the modeling and control framework onto real robot hardware.

9. Conclusions

This paper has investigated dynamic modeling and cooperative trajectory-tracking control for serially assembled reconfigurable miniature modular robotic swarms intended for payload transportation. Instead of rebuilding complete global system matrices when robot units are added or removed, the presented hierarchical nested recursive constraint-following framework based on UK theory only updates local constraint relations, which is well suited for variable-scale underactuated modular clusters. Numerical simulations on a four-robot transportation swarm yield several key scientific findings. First, tracking errors originating from inconsistent initial module poses converge to near zero within 0.5s, and high-precision heading synchronization between serially connected units can be guaranteed. Second, comparative simulations against the LQR baseline controller show that the nested constraint-following strategy produces smaller peak tracking error and markedly lower cumulative error across all robot modules. Third, under external torque disturbance, the swarm retains stable cooperative motion; control torques exhibit limited transient fluctuations and quickly return to steady states after disturbance removal, confirming competitive disturbance-rejection capability. Numerical tests for an eight-robot serial transportation swarm further illustrate the scalability potential of the hierarchical nested constraint-following strategy as the number of connected modules increases.

This study provides a unified modeling and coordination-control solution for reconfigurable micro-robotic transport platforms. For future work, physical prototype experiments will be conducted to validate the presented approach. Moreover, reconfigurable assembly topologies of higher complexity and anti-disturbance control performance will be further investigated to advance the practical deployment of micro-modular swarm transportation systems.

Author Contributions: X.S. developed the conceptualization and methodology and finished the manuscript. F.X. contributed the simulation. D.L. and J.H. provided guidance. All authors have read and agreed to the published version of the manuscript.

Funding: Supported by the National Natural Science Foundation of China (Grant No. 52575005), the Hebei Provincial Major Science and Technology Support Plan (Grant No. 262X1901D), and the Key Laboratory of IoT Monitoring and Early Warning, Ministry of Emergency Management, Project "Vice President of Science and Technology" of Changping District, Beijing.

Institutional Review Board Statement: Not applicable.

Informed Consent Statement: Not applicable.

Data Availability Statement: Data will be made available upon request.

Acknowledgments: We would like to express our sincere gratitude to Ye-Hwa Chen and Yonghua Huang for their valuable advice and contributions during the development process, especially regarding the simulation and control of robots.

Conflicts of Interest: The authors declare no conflicts of interest.

Abbreviations

The following abbreviations are used in this manuscript:

Symbol	Description
M	System inertia matrix
$q, \dot{q}, \ddot{q}$	Generalized coordinate, velocity and acceleration vector
Q	Generalized impressed force vector
Q^e	Generalized constraint force vector
A	Constraint matrix
b	Constraint right-hand side vector
$(\cdot)^+$	Moore-Penrose generalized inverse
m	Mass of single robot module
I_z	Yaw moment of inertia
x, y	Cartesian position coordinates
φ	Heading angle
δ	Front-wheel steering input
Abbreviations	
τ	Control input vector
κ	Damping correction gain
UK	Udwadia–Kalaba
LQR	Linear Quadratic Regulator

Appendix A

Proof of Theorem 1. (i) After C_1 is imposed, the constrained mechanical system S is

$$S : M\ddot{q} = Q_0 + M^{\frac{1}{2}}\bar{\mathbf{B}}_1^+(\bar{\mathbf{b}}_1 - \bar{\mathbf{B}}_1 M^{-\frac{1}{2}} Q_0) =: Q_1 \tag{A1}$$

where
$Q_0 = \begin{bmatrix} Q_{01} \\ Q_{02} \end{bmatrix}, \bar{\mathbf{b}}_1 = \begin{bmatrix} \bar{b}_1 \\ 0 \end{bmatrix}, \bar{\mathbf{B}}_1 = \bar{\mathbf{A}}_1 M^{-\frac{1}{2}}, \bar{\mathbf{A}}_1 = \begin{bmatrix} \bar{A}_1 & 0 \\ 0 & 0 \end{bmatrix}.$
Imposing C_2, we have the constrained system given by

$$S : M\ddot{q} = Q_1 + M^{\frac{1}{2}}\bar{\mathbf{B}}_2^+(\bar{\mathbf{b}}_2 - \bar{\mathbf{B}}_2 M^{-\frac{1}{2}} Q_1) =: Q_2 \tag{A2}$$

where
$\bar{\mathbf{b}}_2 = \begin{bmatrix} 0 \\ \bar{b}_2 \end{bmatrix}, \bar{\mathbf{B}}_2 = \bar{\mathbf{A}}_2 M^{-\frac{1}{2}}, \bar{\mathbf{A}}_2 = \begin{bmatrix} 0 & 0 \\ 0 & \bar{A}_2 \end{bmatrix}.$

The system (A2) meets C_2. We now check whether it meets C_1. Premultiplying both sides of (A2) by $\bar{\mathbf{A}}_1 M^{-1}$ yields

$$\begin{aligned}
\bar{\mathbf{A}}_1 M^{-1} M\ddot{q} &= \bar{\mathbf{A}}_1 M^{-1} Q_2 \\
&= \bar{\mathbf{A}}_1 M^{-1} Q_1 + \bar{\mathbf{A}}_1 M^{-1} M^{\frac{1}{2}} \bar{\mathbf{B}}_2^{+} (\bar{\mathbf{b}}_2 - \bar{\mathbf{B}}_2 M^{-\frac{1}{2}} Q_1) \\
&= \bar{\mathbf{A}}_1 M^{-1} Q_1 + \bar{\mathbf{A}}_1 M^{-\frac{1}{2}} \bar{\mathbf{B}}_2^{+} (\bar{\mathbf{b}}_2 - \bar{\mathbf{B}}_2 M^{-\frac{1}{2}} Q_1) \\
&= \bar{\mathbf{A}}_1 M^{-1} Q_1 + \underbrace{\bar{\mathbf{A}}_1 M^{-\frac{1}{2}} (\bar{\mathbf{A}}_2 M^{-\frac{1}{2}})^{+} (\bar{\mathbf{b}}_2 - \bar{\mathbf{A}}_2 M^{-\frac{1}{2}} M^{-\frac{1}{2}} Q_1)}_{equation 15} \\
&= \bar{\mathbf{A}}_1 M^{-1} Q_1 + 0 \\
&= \bar{\mathbf{b}}_1
\end{aligned} \tag{A3}$$

After C_1 and C_2 are imposed, we have (A2). As $\mathbf{C}$ is imposed, we have (with $\mathbf{B} = \mathbf{A} M^{-\frac{1}{2}}$)

$$S : M\ddot{q} = Q_2 + M^{\frac{1}{2}} \bar{\mathbf{B}} (\bar{\mathbf{b}} - \bar{\mathbf{B}} M^{-\frac{1}{2}} Q_2) =: Q \tag{A4}$$

We know this system S in (A4) meets $\mathbf{C}$. To verify whether S meets C_2, we premultiply (A4) by $\bar{\mathbf{A}}_2 M^{-1}$.

$$\begin{aligned}
\bar{\mathbf{A}}_2 M^{-1} M\ddot{q} &= \bar{\mathbf{A}}_2 M^{-1} Q \\
&= \bar{\mathbf{A}}_2 M^{-1} Q_2 + \bar{\mathbf{A}}_2 M^{-\frac{1}{2}} \bar{\mathbf{B}} (\bar{\mathbf{b}} - \bar{\mathbf{B}} M^{-\frac{1}{2}} Q_2) \\
&= \bar{\mathbf{A}}_2 M^{-1} Q_2 + \underbrace{\bar{\mathbf{A}}_2 M^{-\frac{1}{2}} (\bar{\mathbf{A}} M^{-\frac{1}{2}})^{+} (\bar{\mathbf{b}} - \bar{\mathbf{A}} M^{-\frac{1}{2}} M^{-\frac{1}{2}} Q_2)}_{equation 16} \\
&= \bar{\mathbf{A}}_2 M^{-1} Q_2 + 0 \\
&= \bar{\mathbf{b}}_2
\end{aligned} \tag{A5}$$

Thus, we show that system S in (A4) meets C_2.
To verify if S in (A4) meets C_1, we premultiply (A4) by $\bar{\mathbf{A}}_1 M^{-1}$.

$$\begin{aligned}
\bar{\mathbf{A}}_1 M^{-1} M\ddot{q} &= \bar{\mathbf{A}}_1 M^{-1} Q \\
&= \bar{\mathbf{A}}_1 M^{-1} Q_2 + \bar{\mathbf{A}}_1 M^{-\frac{1}{2}} \bar{\mathbf{B}} (\bar{\mathbf{b}} - \bar{\mathbf{B}} M^{-\frac{1}{2}} Q_2) \\
&= \bar{\mathbf{A}}_1 M^{-1} Q_2 + \underbrace{\bar{\mathbf{A}}_1 M^{-\frac{1}{2}} (\bar{\mathbf{A}} M^{-\frac{1}{2}})^{+} (\bar{\mathbf{b}} - \bar{\mathbf{A}} M^{-\frac{1}{2}} M^{-\frac{1}{2}} Q_2)}_{equation 17} \\
&= \bar{\mathbf{A}}_1 M^{-1} Q_2 + 0 \\
&= \bar{\mathbf{A}}_1 M^{-1} Q_1 + \underbrace{\bar{\mathbf{A}}_1 M^{-\frac{1}{2}} (\bar{\mathbf{A}}_2 M^{-\frac{1}{2}})^{+} (\bar{\mathbf{b}}_2 - \bar{\mathbf{A}}_2 M^{-\frac{1}{2}} M^{-\frac{1}{2}} Q_1)}_{equation 15} \\
&= \bar{\mathbf{A}}_1 M^{-1} Q_1 + 0 \\
&= \bar{\mathbf{b}}_1
\end{aligned} \tag{A6}$$

Thus, we show that system S in (A4) meets C_1. □

References

1. Jia, L.; Su, G.; Zhang, M.; Wen, Q.; Wang, L.; Li, J. Propulsion mechanisms in magnetic microrobotics: From single microrobots to swarms. *Micromachines* **2025**, *16*.
2. Annika Stensson Trigell, J.P.; Rothhämel, M.; Kural, K. Advanced vehicle dynamics of heavy trucks with the perspective of road safety. *Veh. Syst. Dyn.* **2017**, *55*, 1572–1617.
3. Gorelov, V.; Komissarov, A.; Miroshnichenko, A. 8 x 8 wheeled vehicle modeling in a multibody dynamics simulation software. *Procedia Eng.* **2015**, *129*, 300–307.
4. Yubiao Zhang, H.W.; Huang, Y.; Khajepour, A. A comparative study of equivalent modelling for multi-axle vehicle. *Veh. Syst. Dyn.* **2018**, *56*, 443–460.

5. Keller, A.; Sayakhov, V.; Aliukov, S. Simulation Modeling of the Multi-Axle Truck Dynamics. In Proceedings of the World Congress on Engineering, London, UK, 5–7 July 2017; Volume 2.
6. Michalek, M.M. Modular approach to compact low-speed kinematic modelling of multi-articulated urban buses for motion algorithmization purposes. In Proceedings of the 2019 IEEE Intelligent Vehicles Symposium (IV), Paris, France, 9–12 June 2019; pp. 2060–2065.
7. Zhang, A.K.Y.; Huang, Y. Multi-axle/articulated bus dynamics modeling: A reconfigurable approach. *Veh. Syst. Dyn.* **2018**, *56*, 1315–1343.
8. Udwadia, F.E.; Kalaba, R.E. Nonideal constraints and lagrangian dynamics. *J. Aerosp. Eng.* **2000**, *13*, 17–22.
9. Udwadia, F.E.; Kalaba, R.E. A new perspective on constrained motion. *Proc. R. Soc. London. Ser. A Math. Phys. Sci.* **1992**, *439*, 407–410.
10. Udwadia, F.E.; Kalaba, R.E. On the foundations of analytical dynamics. *Int. J. Non-Linear Mech.* **2002**, *37*, 1079–1090.
11. Udwadia, F.E.; Kalaba, R.E. Equations of motion for mechanical systems. *J. Aerosp. Eng.* **1996**, *9*, 64–69.
12. Kalaba, R.; Udwadia, F. Equations of Motion for Nonholonomic, Constrained Dynamical Systems via Gauss's Principle . *J. Appl. Mech.* **1993**, *60*, 662–668.
13. Huang, J.; Chen, Y.H.; Guo, K. Novel approach to multibody system modeling: Cascading and clustering. *J. Aerosp. Eng.* **2014**, *27*, 279–290.
14. Li, X.; Gong, X.; Chen, Y.H.; Huang, J.; Zhong, Z. Integrated path planning-control design for autonomous vehicles in intelligent transportation systems: A neural-activation approach. *IEEE Trans. Intell. Transp. Syst.* **2024**, *25*, 7602–7618.
15. Su, X.; Li, D.; Wei, J.; Liu, Y.; Fan, L.; Chang, X.; Huang, J. A novel approach to nested closed-form dynamics modeling and recursive planning for modular distributed electric drive vehicles. In Proceedings of the 2024 IEEE International Conference on Progress in Informatics and Computing (PIC), Shanghai, China, 20–22 December 2024; pp. 171–176.
16. Su, X.; Li, D.; Fan, L.; Hao, W.; Huang, J. Satisfying boundaries while constraining performance for underactuated mechanical systems control: A novel constraint-following approach. *Chin. J. Mech. Eng.* **2026**, *39*, 100123.
17. Chen, Y.H. Constraint-following servo control design for mechanical systems. *J. Vib. Control* **2009**, *15*, 369–389.
18. Chen, Y.H.; Zhang, X. Adaptive robust approximate constraint-following control for mechanical systems. *J. Frankl. Inst.* **2010**, *347*, 69–86.
19. Zhang, B.; Chen, Y.H.; Jia, Y.; Huang, J.; Yang, D.; Zhong, Z. Accuracy and safety: Tracking control of heavy-duty cooperative transportation systems using constraint-following method. *IEEE Trans. Intell. Transp. Syst.* **2024**, *25*, 3628–3641.
20. Sun, H.; Zhao, H.; Zhen, S.; Huang, K.; Zhao, F.; Chen, X.; Chen, Y.H. Application of the udwadia-kalaba approach to tracking control of mobile robots. *Nonlinear Dyn.* **2015**, *83*, 389–400.

Disclaimer/Publisher's Note: The statements, opinions and data contained in all publications are solely those of the individual author(s) and contributor(s) and not of MDPI and/or the editor(s). MDPI and/or the editor(s) disclaim responsibility for any injury to people or property resulting from any ideas, methods, instructions or products referred to in the content.